ACS APPLIED ENERGY MATERIALS
Cite This: ACS Appl. Energy Mater. 2019, 2, 6904−6910
Article
www.acsaem.org

A Semisolid Electrolyte for Flexible Zn-Ion Batteries

Yanying Lu,[†] Tianyu Zhu,[‡] Nansheng Xu,[†] and Kevin Huang*[,†]

[†]Department of Mechanical Engineering and [‡]Department of Chemistry, University of South Carolina, Columbia, South Carolina 29201, United States

Supporting Information

ABSTRACT: Mechanically strong, ionically conductive, and operationally safe electrolytes are of paramount importance to flexible and wearable electronics. Herein, we report a three-dimensional, double-cross-linked gelatin and sodium alginate hydrogel imbibed with $ZnSO_4$ aqueous solution as an electrolyte membrane for flexible Zn-ion batteries. We show that the designed polymer electrolyte membrane exhibits superior properties in ionic conductivity, mechanical flexibility, electrochemical stability, and compatibility with the Zn anode. The resultant Zn-ion battery outperforms the baseline liquid counterpart in capacity, rate capability, and cycle stability, making it a promising electrolyte membrane candidate for flexible batteries for wearable electronics.

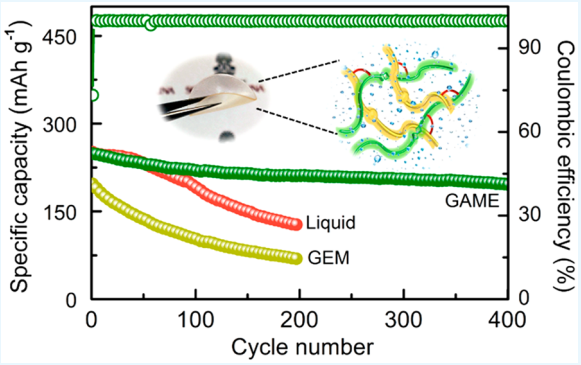

KEYWORDS: *three-dimensional polymeric network, flexibility, ionic conductivity, semisolid electrolyte, aqueous Zn-ion batteries*

The recent high demand for wearable electronics has called for a rapid development of long-life, flexible, and high-safety power sources.[1−3] Rechargeable aqueous Zn-ion batteries (ZIBs) stand out for this application due to their high theoretical volumetric capacity (5854 mAh cm^{-3}), fast charge/discharge rate, low toxicity, and inherent safety.[4−6] However, traditional ZIBs with liquid electrolytes are vulnerable to Zn-dendrite attack and electrolyte leakage, which not only affects battery performance but also causes safety concerns.[7,8] Conventional solid electrolytes consisting of ceramic or polymer materials are either too brittle or less conductive, making them unsuitable for wearable batteries (WBs).[9,10] In comparison, semisolid polymer electrolytes (SSPEs) comprised of an expandable polymer network imbibed with adjustable amounts of electrolyte solution possess a solid-like structure but with liquid-like ionic conductivity, thus making it a better alternative for WB applications.[11−15]

In the literature, Li^+- and Na^+-conducting SSPEs are widely reported.[16−18] In comparison, there are fewer reports on Zn^{2+}-conducting SSPEs. Earlier studies on ZIB-SSPEs are mainly focused on polymer hosts such as poly(ethylene oxide) (PEO),[19] poly(vinylidene fluoride-*co*-hexafluoropropylene) (PVDF−HFP),[20] and poly(vinyl alcohol) (PVA)[21] filled with aqueous Zn salts. Unfortunately, these electrolyte membranes have either low ionic conductivity or poor mechanical strength. A recent interesting development in ZIB-SSPEs is the use of gelatin (GE) as a polymer matrix to host aqueous Zn salts. Derived from collagens, GE is a biocompatible, hydrophilic polymer widely used in food (e.g., chewing candies) and pharmaceutical (e.g., pill capsule) industries.[22,23] A main drawback for GE to be a host matrix is, however, its low mechanical strength. To address this issue, cryogenically prepared gelatin hydrogel and polyacrylamide (PAM)-grafted gelatin reinforced by electrospun polyacrylonitrile fibers have been explored.[24,25] The enhanced electrochemical and mechanical properties have inspired the exploration of more effective ways to improve GE-based membranes for practical WBs. Another well-known gel forming biopolymer is sodium alginate (SA). Because of its high modulus, high concentration of polar groups, and easy cross-linking with cations,[26,27] SA is also considered a potential candidate as a membrane material.

Here we report a three-dimensional (3D), double-cross-linked hydrogel derived from GE and sodium alginate (SA) as the host for Zn-ion conduction. Our approach to developing a flexible and robust Zn^{2+}-SSPE membrane is to leverage the advantages of GE and SA, i.e., the hydrophilicity of GE as well as high dielectric strength and high modulus of SA, through two cross-linking reactions to form an interpenetrating 3D network with ample polar groups (carboxyl and hydroxyl) that can facilitate the dissociation of inorganic salts and immobilize the electrolyte solution. More importantly, the strong covalent bonding and reversible ionic and hydrogen bonding are coexistent within the dual network, which provides the membrane with flexibility, toughness, self-healing ability, and thermal stability. Previous research on GE/SA hybrid has primarily focused on tissue engineering scaffolds (e.g., regeneration of tooth, bone, and skin).[28,29] To the best of our knowledge, our work is the first demonstration of GE/SA cross-linked hybrid membrane as a flexible, tough, and yet

Received: July 21, 2019
Accepted: September 4, 2019
Published: September 4, 2019

DOI: 10.1021/acsaem.9b01415
ACS Appl. Energy Mater. 2019, 2, 6904−6910

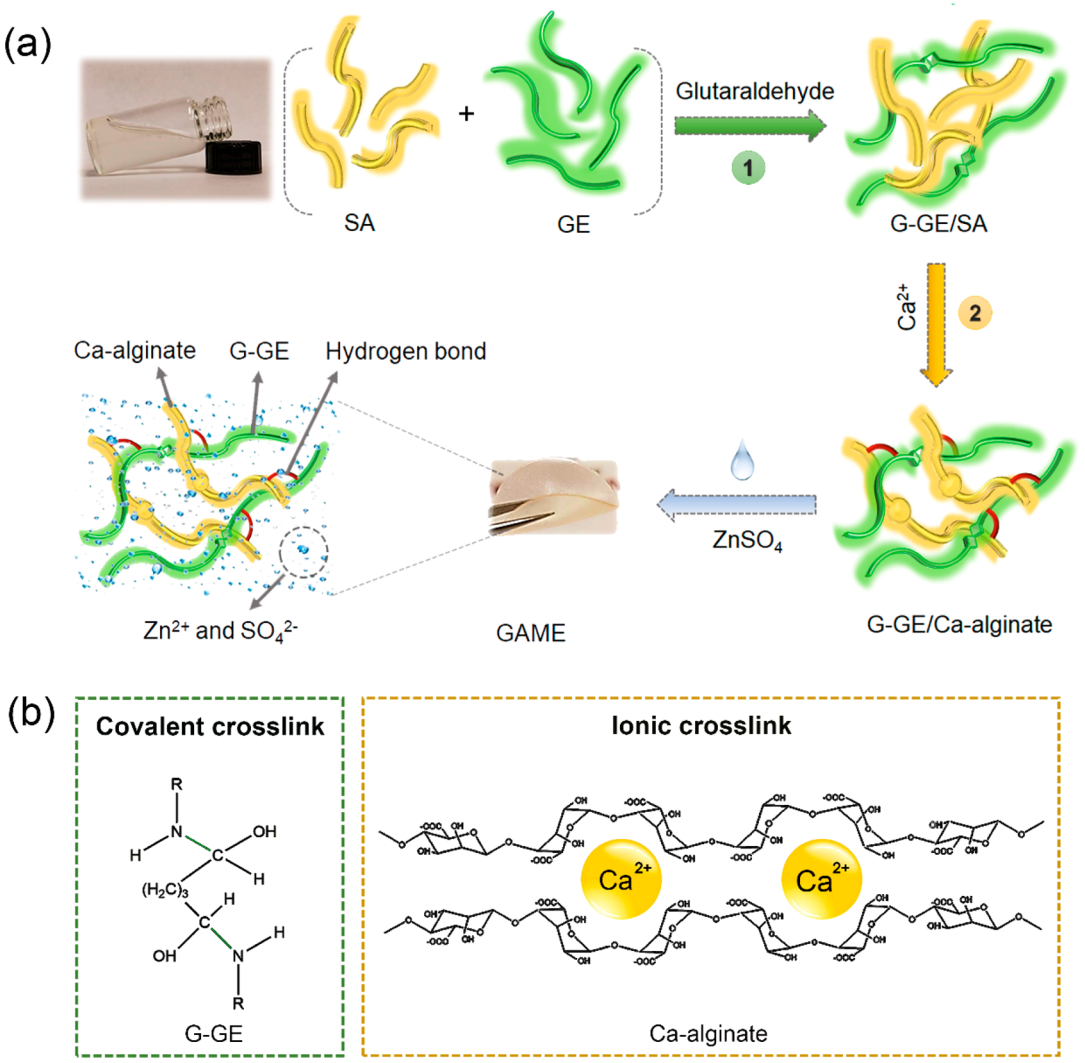

Figure 1. (a) Schematic of the overall process to make GAME. (b) Cross-linked polymers of G-GE (GE cross-link with glutaraldehyde) and Ca-alginate (SA cross-link with $CaCl_2$).

biocompatible polymer electrolyte host for potential WB applications.

The basic synthesis procedure and the corresponding cross-linking reactions are shown in Figure 1 for the gelatine- and alginate-based membrane electrolyte (denoted as GAME). The first cross-linking reaction takes place between GE and glutaraldehyde (Figure S1a), where the amine groups in GE are covalently bonded with the aldehyde groups in glutaraldehyde,[30,31] forming a cross-linked GE hydrogel (denoted as G-GE). The covalent bonding has strong interactions, which enhances the mechanical strength. Next, an ionically cross-linking reaction takes place between SA and $CaCl_2$ via ion exchange (Figure S1b). Many multivalent cations have been investigated to cross-link with SA, but most of them (e.g., Pb, Cu, Cd, and Ba) are too toxic.[32,33] Selection of Ca^{2+} for cross-linking cation represents a balance between affinity and environmentally friendliness. After ionic cross-linking with Ca^{2+}, the blocks in SA chains form a network microstructure (denoted as Ca-alginate), providing a robust scaffold for Zn-ion transport after electrolyte uptake. On the other hand, it is reported that the ionic bonding in the polymer is a dynamic and reversible interaction, which could break and dissipate energy during stretching and self-healing upon unloading, thus ensuring a good stretchability of the polymer matrix.[34] After imbibing in $ZnSO_4$ solution, the membrane finally transforms into a flexible Zn-ion conducting electrolyte. Based on the unique properties derived from GE-SA cross-linking reactions, the following advantages are expected for the GAME: (1) the abundant hydrophilic functional hydroxyl and carboxylic groups on the polymer chains facilitate $ZnSO_4$ absorption and dissociation; (2) the interpenetrated 3D network not only provides the material with high mechanical strength but also ensures more liquid electrolyte uptake; and (3) the rigid covalent bonding can dissipate mechanical energy induced by deformation, while the reversible ionic bonding together with hydrogen bonding and chain entanglements between the two polymers allow a quick recovery after the deformation. Therefore, it is expected that the new GAME electrolyte will exhibit both good mechanical and electrochemical performances.

The mass ratio of GE and SA in GAME was optimized based on mechanical strength, phase composition, and ionic conductivity. For comparison, a pure GE membrane (denoted as GEM) and SA membrane (denoted as SAM) were also prepared by imbibing in a 2 M $ZnSO_4$ solution. Figure 2a shows the stress−strain curves of GEM and GAME at different

DOI: 10.1021/acsaem.9b01415
ACS Appl. Energy Mater. 2019, 2, 6904−6910

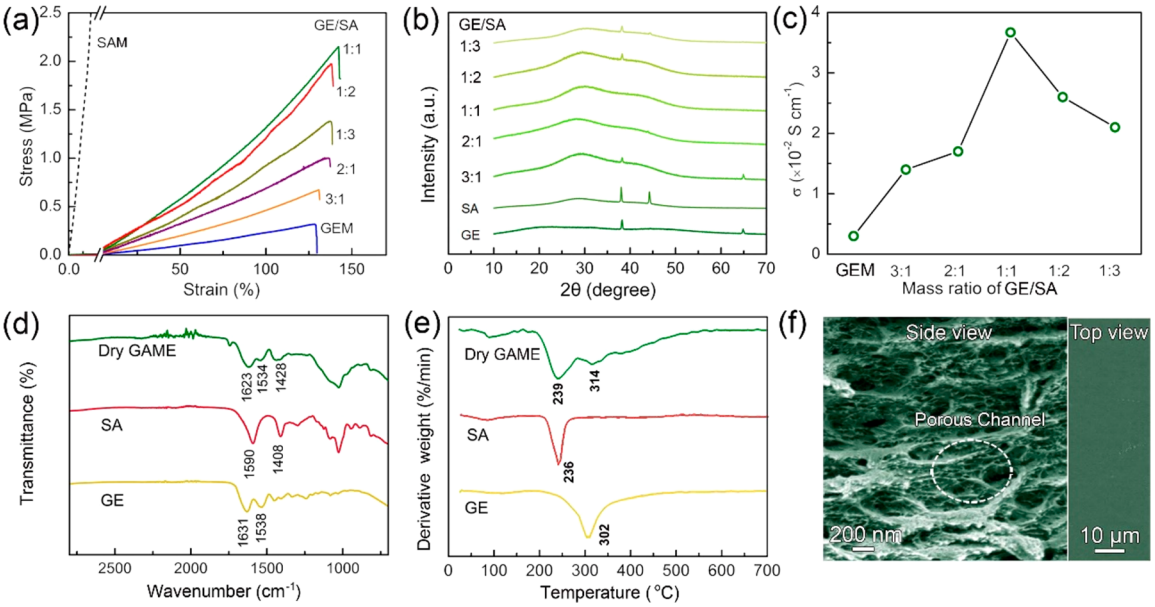

Figure 2. Optimal GE/SA ratio and physiochemical properties of the GAME. (a) Stress−strain curves of SAM, GEM, and GAME. (b) XRD patterns of GE, SA, and dry GAME. (c) Ionic conductivity of GEM and GAME. (d) FTIR spectra of GE, SA, and dry GAME at GE/SA = 1/1. (e) DTG analysis of GE, SA, and dry GAME at GE/SA = 1/1. (f) SEM image of dry GAME at GE/SA = 1/1 with different views.

GE/SA mass ratios. As expected, the pure SAM is tough and rigid. Once mixed with the softer GEM and went through the cross-link reactions, the GAME behavors more like a plastic, but with much higher strength than the pure GEM. The latter is expcted from the synergetic contributions between the cross-linked polymers discussed above. The highest tensile strength, 2.14 MPa, of the GAME is observed at GE/SA = 1/1, which is almost 1 order of magnitude higher than 0.32 MPa of GEM.

The phase evolution of the dry-GAME with different GE/SA mass ratios is shown in Figure 2b of XRD patterns. Because SA disrupts the alignment of GE chains, the peak intensity of GE continuously decreases with increasing SA content. At GE/SA = 1/1, the dry-GAME is predominantly amorphous. At either GE/SA < 1/1 or >1/1, the crystalline peaks of SA or GE gradually appear, implying that excess SA or GE disrupts the GE-SA interactions. According to previous research,[35,36] the amorphous voids could facilitate more liquid electrolyte uptake. Therefore, Figure 2c shows that the GE/SA = 1/1 with the highest degree of amorphousness exhibits the highest ionic conductivity of 3.7×10^{-2} S cm^{-1}, which represents a marked enhancement over other ZIB-SSPEs reported (Table S1).

To understand the internal molecular interactions within the optimal GAME composition (GE/SA = 1/1), FTIR spectra were performed. Figure S2 shows FTIR spectra of SA and GE accompanied by their cross-link products of Ca-alginate and G-GE, respectively. The obvious band shift and strength change of the characteristic peaks confirm the successful cross-link reaction of SA with Ca^{2+} ions and GE with glutaraldehyde. The FTIR spectra of GE, SA, and dry-GAME are further compared in Figure 2d. After the cross-link reaction, $-COO^-$ stretching at 1408 cm^{-1} in SA shifts to higher wavenumber of 1428 cm^{-1} in dry-GAME, implying the presence of ionic bonding between $-COO^-$ and Ca^{2+}.[37−39] Contrary to the peak shifts observed in GE to G-GE conversion (Figure S2b), the band at 1538 cm^{-1} in GE decreases to 1534 cm^{-1} in dry-GAME, which mainly due to the hydrogen bonds formed between $-COO^-$ groups in Ca-alginate and $-CONH_2$ groups in G-GE.[29,40] Furthermore, the broad peak centered at about 1623 cm^{-1} in dry-GAME could also be attributed to the peak overlaps of amide in G-GE and $-COO^-$ in Ca-alginate.[41] Overall, the FTIR results provide a strong evidence for the intermolecular interactions and good molecular compatibility between SA and GE.

The thermal stability of GAME was also analyzed by thermogravimetric analysis (TGA). Figure 2e shows differential thermal gravimetry (DTG) data of GE, SA, and dry-GAME. The initial fluctuations of the three samples before 200 °C are mainly due to the adsorbed moisture. The peak at 236 °C for SA is related to its decomposition and formation of intermediate product (Na_2CO_3),[38] while the peak at 302 °C for GE is due to its decomposition and loss of ammonia.[42] In comparison, the thermal decomposition temperatures in dry-GAME increase to 239 and 314 °C, respectively. This implies the formation of stronger bonding within the polymers and therefore a better stability in GAME.[37]

Figure 2f shows SEM images of the optimal GAME (GE/SA = 1/1) after freeze-drying. From the cross-sectional view, it is clear to observe that the interconnected porous channels within the network are formed. Such a porous structure is favorable to imbibe more electrolyte solutions and thus to achieve a high ionic conductivity, as demonstrated in Figure 2c and further confirmed by the maximal water uptake (219%, see Figure S3). Additionally, a flat and smooth surface is observed from the top view. Atomic force microscopy (AFM) image confirms that its surface roughness is only ∼16 nm (Figure S4). For the solid−solid interface in this system, the smooth surface is necessary to ensure a low GAME/electrode contact resistance and promote ion transport.[43] In comparison, nonoptimal dry-GAMEs (e.g., GE/SA = 3/1 and 1/3) exhibit a higher degree of surface roughness, severer particle aggregation/segregation, and more compacted texture (Figure S5), which leads to a weaker mechanical strength (Figure 2a), less water uptake (Figure S3), and lower ionic conductivity (Figure 2c). Hence, GAME with mass ratio of GE/SA = 1/1 was selected for further electrochemical tests in ZIBs.

DOI: 10.1021/acsaem.9b01415
ACS Appl. Energy Mater. 2019, 2, 6904−6910

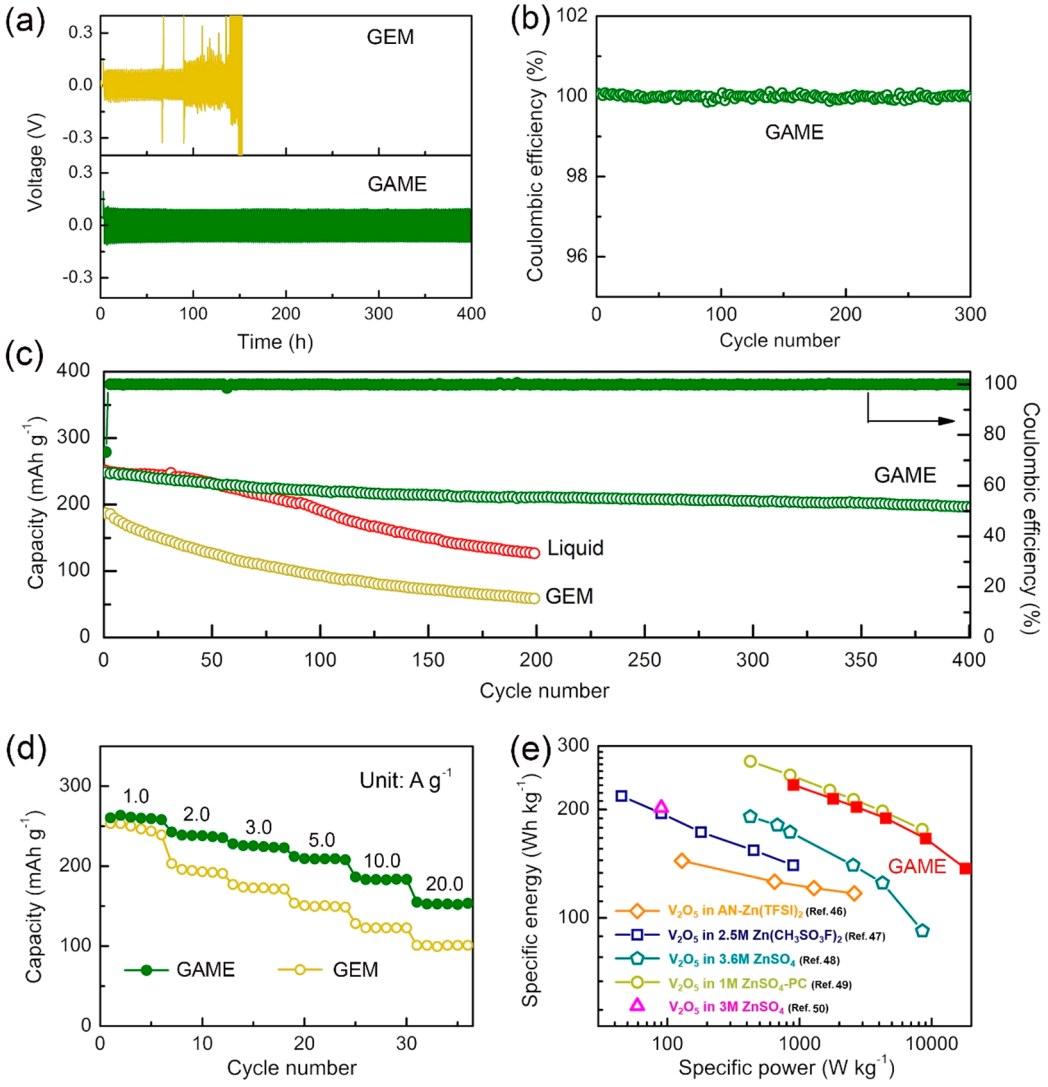

Figure 3. (a) Cyclic performance of GAME and GEM electrodes at 0.5 mA cm^{-2}. (b) Coulombic efficiency of GAME measured at 1.0 mA cm^{-2} for 1.0 mAh cm^{-2}. (c) Comparison of the cyclic stability among three different electrolytes at 2.0 A g^{-1}. (d) Rate capability of the GAME cells at various current densities. (e) Ragone plot of GAME-ZIB compared with other ZIBs.

The compatibility of the selected GAME with Zn anode was first evaluated by symmetric cells. Figure 3a compares the plating/stripping cycles at 0.5 mA cm^{-2} between GAME and GEM. The GEM cell experiences a gradual increase in voltage oscillations and ultimately fails due to the Zn-dendrite attack. In comparison, the GAME cell shows stable cycles with negligible voltage fluctuation for 400 h. The better stability of Zn plating/stripping with GAME is further supported by Figure 3b, where a stable Coulombic efficiency vs cycle is shown at a higher current density of 1.0 mA cm^{-2} for 300 cycles. The outstanding plating/stripping performance of GAME is attributed to its flexibility and toughness, which can accommodate the volume change during Zn deposition, thus suppressing the growth of Zn dendrites. In contrast, the GEM with lower mechanical strength can hardly suppress the growth of dendritic Zn during long cycling, leading to fast failure of the battery. Moreover, linear sweep voltammograms in Figure S6 show that GAME gives a broader voltage window than that of the GEM (2.1 V vs 1.6 V). To better understand the nature of Zn-ion transport, the dependence of conductivity on temperature is plotted for GAME and GEM in Figure S7. The ionic conductivity follows the Arrhenius relationship from 30 to 70 °C. The activation energy (E_a) is 18.9 kJ mol^{-1} for GEM and only 9.9 kJ mol^{-1} for GAME. The considerably lower E_a infers that the Zn ion is much easier to transport in GAME than GEM.

To demonstrate the performance of GAME in a practical ZIB, full cells were assembled with V_2O_5/CNT nanocomposite as cathode and Zn metal as anode. V_2O_5 is selected as the cathode due to its layered structure suitable for Zn^{2+} storage. Note that we recognize that this is not the best ZIB cathode developed so far. Many works have been reported to improve the V_2O_5 electrochemical performance by expanding interlayer, creating mixed valence, avoiding cations intercalation, and involving crystal water.[44] Here in this study, as our goal is to demonstrate a new electrolyte membrane for flexible and wearable batteries, we prepared the V_2O_5 by a common method used it to evaluate our electrolyte membrane and compared with the liquid electrolyte performance. The XRD patterns, Raman spectra, and SEM image accompanied by EDS mapping confirm the formation of V_2O_5/CNT nanocomposite, where V_2O_5 nanowires with a diameter of 80−120 nm are

DOI: 10.1021/acsaem.9b01415
ACS Appl. Energy Mater. 2019, 2, 6904−6910

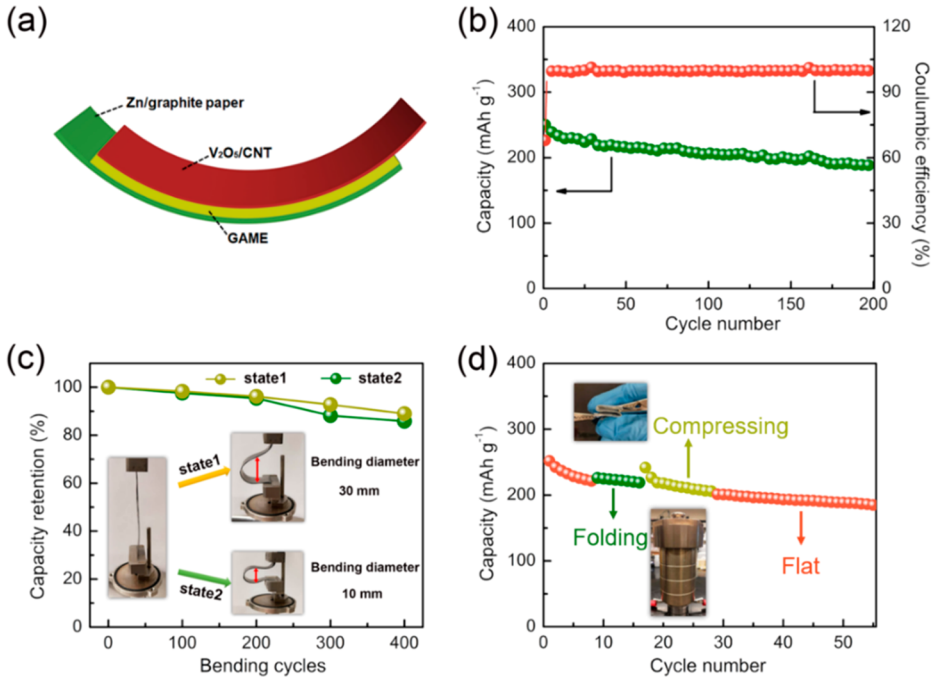

Figure 4. Configuration and performance of a flexible semisolid Zn/V_2O_5 battery. (a) Schematic diagram of a flexible semisolid Zn/V_2O_5 battery. (b) Cyclic performance at 2.0 A g^{-1}. (c) Capacity retention vs bending cycle at 2.0 A g^{-1}. The insets show photographs of the battery under two bending states. (d) Cyclic performance under various mechanical stimuli at 2.0 A g^{-1}.

intertwined with CNT in a diameter of ~30 nm (Figures S8–S11).[45] The cyclic stabilities of GAME, GEM, and liquid electrolyte are compared in Figure 3c. The GEM cell exhibits a relatively low capacity with a fast decay; after 200 cycles, it retains a capacity of only 69 mAh g^{-1} (~35% retention rate) at 2 A g^{-1}. At the same current density, the liquid electrolyte cell exhibits a higher capacity of 127 mAh g^{-1} (~51% retention) after 200 cycles. In contrast, the GAME cell shows the highest capacity of 212 mAh g^{-1} after 200 cycles (~85% retention), and the capacity retains at 79% even after 400 cycles. The SEM images of the Zn anode from the GAME and liquid electrolyte cells after cycles are shown in Figure S12. Upon comparison with the liquid electrolyte cell, where the Zn anode exhibits a severe surface morphological change, the intactness of the Zn anode in the GAME cell implies that Zn dendrite may have been effectively suppressed, resulting in its better cyclic stability.

The rate capabilities of GAME- and GEM-based cells are compared in Figure 3d in a current density range of 1.0–20 A g^{-1}. As expected, the GAME cell demonstrates a better rate performance than the GEM cell, i.e., 260 vs 253 mAh g^{-1} at 1.0 A g^{-1} and 152 vs 101 mAh g^{-1} at 20.0 A g^{-1}. The relatively inferior rate capability of the GEM cell is mainly attributed to its lower ionic conductivity and poorer interfacial contacts with electrodes. Compared to liquid-electrolyte-based ZIB cells with V_2O_5 cathodes synthesized by different methods,[46−50] Figure 3e of the Ragone plot shows that the GAME-based ZIB cell is among the top performers. The better rate and cyclic performance of the GAME cell are believed to arise from (1) a flat and smooth surface ensuring a good interfacial contact between electrodes and GAME; (2) 3D cross-linked network with rich functional groups providing good ionic conductivity; and (3) the strong interactions of the polymers offering both elasticity and toughness for a better resistance to Zn-dendrite attacks. On the basis of above advantages, it is reasonable to expect that the GAME-based ZIB will also perform well with recently reported better performing ZIB cathodes.[51−53]

To demonstrate the flexibility, GAME cells with a simple three-layer (i.e., V_2O_5/CNT cathode, GAME electrolyte, and Zn anode) were assembled. Figures S13 and S14 show stable open-circuit voltage under flat, 90°, and 180° angle and nondiscernible discharge curves. Upon connection of the assembled two larger pouch cells in series, Figure S15 shows the lighting of nine light-emitting diodes (LED) even under a 180° bending state. However, there is a concern on permanent mechanical deformation of the thin Zn foil after multiple bending actions. To address this problem, we investigate the use of a flexible graphite paper loaded with Zn, prepared by the electrodeposition method (Figure S16), as an anode. The XRD, SEM, and EDX elemental mapping confirm that the flake-like Zn is uniformly deposited on the graphite papers (Figures S17–S19). Figure 4a schematically shows the battery assembled by sandwiching a GAME electrolyte between the V_2O_5/CNT cathode and Zn/graphite paper anode. The cross-sectional SEM image of the flexible semisolid Zn/V_2O_5 battery is shown in Figure S20. Figure 4b shows the cyclic stability of the flexible battery at 2.0 A g^{-1}, delivering a capacity of 251 mAh g^{-1} at the first cycle and 188 mAh g^{-1} after 200 cycles at a Coulombic efficiency >99.8%. By bending the battery to various states, Figure 4c further shows that 89% and 86% of the original capacity can be preserved after 400 bending cycles at a bending diameter of 30 and 10 mm, respectively. Notably, the SEM image of Figure S20 confirms that the GAME interfacial area is well retained after mechanical bending cycles. The cyclic performance with simultaneous folding and compressing is also tested to further demonstrate the intrinsic elasticity and toughness of the GAME. As depicted in Figure 4d, the cell can undergo folding at a load of 1470× the device weight for 55 cycles, while still retaining 74% of the original capacity. In

DOI: 10.1021/acsaem.9b01415
ACS Appl. Energy Mater. 2019, 2, 6904−6910

addition, the temperature-dependent specific capacity and the corresponding charge/discharge curves of the semisolid Zn/V_2O_5 battery are shown in Figure S22. The battery exhibits a stable reversible capacity as the temperature increases from 10 to 70 °C, indicating that the GAME is well suited to operate at a large temperature window. Overall, these demonstrations show that GAME-ZIBs are flexibile and strong enough for WB applications.

In summary, a strong, flexible and biocompatible polymeric membrane has been successfully synthesized by combining GE and SA with sequential cross-linking reactions. The formed polymeric matrix contains a 3D interpenetrating network, strong intermolecular interactions, and high concentration of hydrophilic functional groups, enabling good mechanical property and thermal/electrochemical stability. When imbibed in aqueous $ZnSO_4$, the highly amorphous, hydrophilic polymer membrane becomes an excellent Zn-ion conductor. The electrochemical evaluations by symmetrical and full cells confirm that the semisolid membrane electrolyte yields a better reversible capacity, rate capability, and cyclic stability, mainly benefiting from its higher conductivity and resistance to Zn-dendrite attack. The flexible battery cell tests under various bending angles, stress states, and mechanical stimuli also demonstrate that the GAME is a robust electrolyte for ZIB-based WB applications.

■ ASSOCIATED CONTENT

Supporting Information

The Supporting Information is available free of charge on the ACS Publications website at DOI: 10.1021/acsaem.9b01415.

List of experimental section, cross-linking reactions of GE with glutaraldehyde and SA with $CaCl_2$, FTIR spectra of SA and Ca-alginate, GE and G-GE, water uptake, AFM image of GAME, SEM image of the freeze-dried GAME, linear sweep voltammograms of the GAME and GEM, Arrhenius plot of the ionic conductivity of GAME and GEM, XRD patterns, Raman spectra, SEM image and EDX elemental mapping of the V_2O_5/CNT nanocomposite, morphology images of Zn anode after 150 cycles in GAME and liquid electrolyte, optical photographs of the flexible ZIB with V_2O_5/CNT cathode, GAME, and Zn/graphite paper anode showing three different bending states of cells, discharge curves of the cell at 1.0 A g^{-1} under flat, bent to 90°, and bent to 180°, an LED array powdered by two pouch cells in series with flat and bent state, schematic diagram of electrodeposition setup, optical photographs of graphite foil before and after Zn deposition, XRD patterns of pure graphite foil, Zn foil, and the electrodeposition Zn/graphite foil, SEM images and EDX elemental mapping of Zn/graphite paper, cross-sectional SEM image of the flexible semisolid Zn/V_2O_5 battery and the location of the bent GAME area, specific capacity and charge/discharge curves of the semisolid Zn/V_2O_5 battery at different temperature at 1 A g^{-1}, comparison of ion conductivities of Zn-ion polymer electrolytes (PDF)

■ AUTHOR INFORMATION

Corresponding Author

*E-mail: huang46@cec.sc.edu.

ORCID

Kevin Huang: 0000-0002-1232-4593

Notes

The authors declare no competing financial interest.

■ ACKNOWLEDGMENTS

The authors thank the National Science Foundation for the financial support with Award CBET-1801284.

■ REFERENCES

(1) Li, T.; Li, Y.; Zhang, T. Materials, Structures, and Functions for Flexible and Stretchable Biomimetic Sensors. *Acc. Chem. Res.* **2019**, *52*, 288−296.

(2) Wu, Z.; Wang, Y.; Liu, X.; Lv, C.; Li, Y.; Wei, D.; Liu, Z. Carbon-Nanomaterial-Based Flexible Batteries for Wearable Electronics. *Adv. Mater.* **2019**, *31*, 1800716.

(3) Xue, L.; Savilov, S. V.; Lunin, V. V.; Xia, H. Self-Standing Porous $LiCoO_2$ Nanosheet Arrays as 3D Cathodes for Flexible Li-Ion Batteries. *Adv. Funct. Mater.* **2018**, *28*, 1705836.

(4) Huang, S.; Wan, F.; Bi, S.; Zhu, J.; Niu, Z.; Chen, J. A Self-Healing Integrated All-in-One Zinc-Ion Battery. *Angew. Chem.* **2019**, *131*, 4357−4361.

(5) Wan, F.; Zhang, L.; Wang, X.; Bi, S.; Niu, Z.; Chen, J. An Aqueous Rechargeable Zinc-Organic Battery with Hybrid Mechanism. *Adv. Funct. Mater.* **2018**, *28*, 1804975.

(6) Xue, L.; Zhang, Q.; Zhu, X.; Gu, L.; Yue, J.; Xia, Q.; Xing, T.; Chen, T.; Yao, Y.; Xia, H. 3D $LiCoO_2$ nanosheets assembled nanorod arrays via confined dissolution-recrystallization for advanced aqueous lithium-ion batteries. *Nano Energy* **2019**, *56*, 463−472.

(7) Wan, F.; Zhang, L.; Dai, X.; Wang, X.; Niu, Z.; Chen, J. Aqueous rechargeable zinc/sodium vanadate batteries with enhanced performance from simultaneous insertion of dual carriers. *Nat. Commun.* **2018**, *9*, 1656.

(8) Wan, F.; Zhang, Y.; Zhang, L.; Liu, D.; Wang, C.; Song, L.; Niu, Z.; Chen, J. *Angew. Chem., Int. Ed.* **2019**, *58*, 7062−7067.

(9) Wei, T.; Gong, Y.; Zhao, X.; Huang, K. An All-Ceramic Solid-State Rechargeable Na^+-Battery Operated at Intermediate Temperatures. *Adv. Funct. Mater.* **2014**, *24*, 5380−5384.

(10) Cho, Y. G.; Hwang, C.; Cheong, D. S.; Kim, Y. S.; Song, H. K. Gel/Solid Polymer Electrolytes Characterized by In Situ Gelation or Polymerization for Electrochemical Energy Systems. *Adv. Mater.* **2019**, *31*, 1804909.

(11) Hu, X.; Li, Z.; Chen, J. Flexible Li-CO_2 Batteries with Liquid-Free Electrolyte. *Angew. Chem., Int. Ed.* **2017**, *56*, 5785−5789.

(12) Cheng, X.; Pan, J.; Zhao, Y.; Liao, M.; Peng, H. Gel Polymer Electrolytes for Electrochemical Energy Storage. *Adv. Energy Mater.* **2018**, *8*, 1702184.

(13) Wang, K.; Zhang, X.; Li, C.; Sun, X.; Meng, Q.; Ma, Y.; Wei, Z. Chemically Crosslinked Hydrogel Film Leads to Integrated Flexible Supercapacitors with Superior Performance. *Adv. Mater.* **2015**, *27*, 7451−7457.

(14) Liu, Z.; Liang, G.; Zhan, Y.; Li, H.; Wang, Z.; Ma, L.; Wang, Y.; Niu, X.; Zhi, C. A soft yet device-level dynamically super-tough supercapacitor enabled by an energy-dissipative dual-crosslinked hydrogel electrolyte. *Nano Energy* **2019**, *58*, 732−742.

(15) Wang, K.; Zhang, X.; Li, C.; Zhang, H.; Sun, X.; Xu, N.; Ma, Y. Flexible solid-state supercapacitors based on a conducting polymer hydrogel with enhanced electrochemical performance. *J. Mater. Chem. A* **2014**, *2*, 19726−19732.

(16) Gao, H.; Zhou, W.; Park, K.; Goodenough, J. B. A Sodium-Ion Battery with a Low-Cost Cross-Linked Gel-Polymer Electrolyte. *Adv. Energy Mater.* **2016**, *6*, 1600467.

(17) Zhou, D.; Chen, Y.; Li, B.; Fan, H.; Cheng, F.; Shanmukaraj, D.; Rojo, T.; Armand, M.; Wang, G. A Stable Quasi-Solid-State Sodium-Sulfur Battery. *Angew. Chem., Int. Ed.* **2018**, *57*, 10168−10172.

DOI: 10.1021/acsaem.9b01415
ACS Appl. Energy Mater. 2019, 2, 6904−6910

(18) Li, H.; Peng, L.; Zhu, Y.; Zhang, X.; Yu, G. Achieving High-Energy-High-Power Density in a Flexible Quasi-Solid-State Sodium Ion Capacitor. *Nano Lett.* **2016**, *16*, 5938−5943.
(19) Silva, M. M.; Smith, M. J.; Lightfoot, P. Characterisation of a Zn Triflate-based Polymer Electrolyte. *Electrochim. Acta* **1999**, *17*, 3−10.
(20) Ye, H.; Xu, J. J. Zinc Ion Conducting Polymer Electrolytes Based on Oligomeric Polyether/PVDF-HFP Blends. *J. Power Sources* **2007**, *165*, 500−508.
(21) Zeng, Y.; Zhang, X.; Meng, Y.; Yu, M.; Yi, J.; Wu, Y.; Lu, X.; Tong, Y. Achieving Ultrahigh Energy Density and Long Durability in a Flexible Rechargeable Quasi-Solid-State Zn-MnO_2 Battery. *Adv. Mater.* **2017**, *29*, 1700274.
(22) Vieira, D. F.; Avellaneda, C. O.; Pawlicka, A. Conductivity Study of a Gelatin-based Polymer Electrolyte. *Electrochim. Acta* **2007**, *53*, 1404−1408.
(23) Choudhury, N. A.; Sampath, S.; Shukla, A. K. Gelatin Hydrogel Electrolytes and Their Application to Electrochemical Supercapacitors. *J. Electrochem. Soc.* **2008**, *155*, A74−A81.
(24) Han, Q.; Chi, X.; Zhang, S.; Liu, Y.; Zhou, B.; Yang, J.; Liu, Y. Durable, Flexible Self-Standing Hydrogel Electrolytes Enabling High-Safety Rechargeable Solid-State Zinc Metal Batteries. *J. Mater. Chem. A* **2018**, *6*, 23046−23054.
(25) Li, H.; Han, C.; Huang, Y.; Huang, Y.; Zhu, M.; Pei, Z.; Xue, Q.; Wang, Z.; Liu, Z.; Tang, Z.; Wang, Y.; Kang, F.; Li, B.; Zhi, C. An Extremely Safe and Wearable Solid-state Zinc Ion Battery Based on a Hierarchical Structured Polymer Electrolyte. *Energy Environ. Sci.* **2018**, *11*, 941−951.
(26) Kovalenko, I.; Zdyrko, B.; Magasinski, A.; Hertzberg, B.; Milicev, Z.; Burtovyy, R.; Luzinov, I.; Yushin, G. A Major Constituent of Brown Algae for Use in High-Capacity Li-Ion Batteries. *Science* **2011**, *334*, 75.
(27) Russo, R.; Malinconico, M.; Santagata, G. Effect of Cross-Linking with Calcium Ions on the Physical Properties of Alginate Films. *Biomacromolecules* **2007**, *8*, 3193−3197.
(28) Venkatesan, J.; Bhatnagar, I.; Manivasagan, P.; Kang, K. H.; Kim, S. K. Alginate Composites for Bone Tissue Engineering: A Review. *Int. J. Biol. Macromol.* **2015**, *72*, 269−281.
(29) Li, Z.; Huang, S.; Liu, Y.; Yao, B.; Hu, T.; Shi, H.; Xie, J.; Fu, X. Tuning Alginate-Gelatin Bioink Properties by Varying Solvent and Their Impact on Stem Cell Behavior. *Sci. Rep.* **2018**, *8*, 8020.
(30) Farris, S.; Song, J.; Huang, Q. Alternative Reaction Mechanism for the Cross-Linking of Gelatin with Glutaraldehyde. *J. Agric. Food Chem.* **2010**, *58*, 998−1003.
(31) Lai, J. Y.; Li, Y. T.; Cho, C. H.; Yu, T. C. Nanoscale Modification of Porous Gelatin Scaffolds with Chondroitin Sulfate for Corneal Stromal Tissue Engineering. *Int. J. Nanomed.* **2012**, *7*, 1101−1114.
(32) Yang, C. H.; Wang, M. X.; Haider, H.; Yang, J. H.; Sun, J. Y.; Chen, Y. M.; Zhou, J.; Suo, Z. Strengthening Alginate/Polyacrylamide Hydrogels Using Various Multivalent Cations. *ACS Appl. Mater. Interfaces* **2013**, *5*, 10418−10422.
(33) Braccini, I.; Pérez, S. Molecular Basis of Ca^{2+}-Induced Gelation in Alginates and Pectins: The Egg-Box Model Revisited. *Biomacromolecules* **2001**, *2*, 1089−1096.
(34) Ma, L.; Chen, S.; Wang, D.; Yang, Q.; Mo, F.; Liang, G.; Li, N.; Zhang, H.; Zapien, J. A.; Zhi, C. Super-Stretchable Zinc-Air Batteries Based on an Alkaline-Tolerant Dual-Network Hydrogel Electrolyte. *Adv. Energy Mater.* **2019**, *9*, 1803046.
(35) Kim, J. I.; Choi, Y.; Chung, K. Y.; Park, J. H. A Structurable Gel-Polymer Electrolyte for Sodium Ion Batteries. *Adv. Funct. Mater.* **2017**, *27*, 1701768.
(36) Fu, J.; Zhang, J.; Song, X.; Zarrin, H.; Tian, X.; Qiao, J.; Rasen, L.; Li, K.; Chen, Z. A Flexible Solid-State Electrolyte for Wide-Scale Integration of Rechargeable Zinc-air Batteries. *Energy Environ. Sci.* **2016**, *9*, 663−670.
(37) Sun, J. Y.; Zhao, X.; Illeperuma, W. R.; Chaudhuri, O.; Oh, K. H.; Mooney, D. J.; Vlassak, J. J.; Suo, Z. Highly Stretchable and Tough Hydrogels. *Nature* **2012**, *489*, 133−136.
(38) da Silva Fernandes, R.; de Moura, M. R.; Glenn, G. M.; Aouada, F. A. Thermal, Microstructural, and Spectroscopic Analysis of Ca^{2+} Alginate/clay Nanocomposite Hydrogel Beads. *J. Mol. Liq.* **2018**, *265*, 327−336.
(39) Liu, J.; Zhang, Q.; Wu, Z. Y.; Wu, J. H.; Li, J. T.; Huang, L.; Sun, S. G. A High-Performance Alginate Hydrogel Binder for the Si/C Anode of a Li-Ion Battery. *Chem. Commun.* **2014**, *50*, 6386−6389.
(40) Kumar, P.; Singh, I. Formulation and Characterization of Tramadol-Loaded IPN Microgels of Alginate and Gelatin: Optimization Using Response Surface Methodology. *Acta Pharm.* **2010**, *60*, 295−310.
(41) Song, L.; Zhu, T.; Yuan, L.; Zhou, J.; Zhang, Y.; Wang, Z.; Tang, C. Ultra-Strong Long-Chain Polyamide Elastomers with Programmable Supramolecular Interactions and Oriented Crystalline Microstructures. *Nat. Commun.* **2019**, *10*, 1315.
(42) Wang, K.; Wang, W.; Ye, R.; Xiao, J.; Liu, Y.; Ding, J.; Zhang, S.; Liu, A. Mechanical and Barrier Properties of Maize Starch-Gelatin Composite Films: Effects of Amylose Content. *J. Sci. Food Agric.* **2017**, *97*, 3613−3622.
(43) Khurana, R.; Schaefer, J. L.; Archer, L. A.; Coates, G. W. Suppression of Lithium Dendrite Growth Using Cross-Linked Polyethylene/Poly(ethylene oxide) Electrolytes: A New Approach for Practical Lithium-Metal Polymer Batteries. *J. Am. Chem. Soc.* **2014**, *136*, 7395−7402.
(44) Zhao, J.; Ren, H.; Liang, Q.; Yuan, D.; Xi, S.; Wu, C.; Manalastas, W.; Ma, J.; Fang, W.; Zheng, Y.; Du, C.-F.; Srinivasan, M.; Yan, Q. High-performance flexible quasi-solid-state zinc-ion batteries with layer-expanded vanadium oxide cathode and zinc/stainless steel mesh composite anode. *Nano Energy* **2019**, *62*, 94−102.
(45) Cheng, J.; Gu, G.; Guan, Q.; Razal, J. M.; Wang, Z.; Li, X.; Wang, B. Synthesis of a Porous Sheet-Like V_2O_5-CNT Nanocomposite Using an Ice-Templating 'Bricks-and-Mortar' Assembly Approach as a High-Capacity, Long Cycle Life Cathode Material for Lithium-Ion Batteries. *J. Mater. Chem. A* **2016**, *4*, 2729−2737.
(46) Senguttuvan, P.; Han, S. D.; Kim, S.; Lipson, A. L.; Tepavcevic, S.; Fister, T. T.; Bloom, I. D.; Burrell, A. K.; Johnson, C. S. A High Power Rechargeable Nonaqueous Multivalent Zn/V_2O_5 Battery. *Adv. Energy Mater.* **2016**, *6*, 1600826.
(47) Hu, P.; Yan, M.; Zhu, T.; Wang, X.; Wei, X.; Li, J.; Zhou, L.; Li, Z.; Chen, L.; Mai, L. Zn/V_2O_5 Aqueous Hybrid-Ion Battery with High Voltage Platform and Long Cycle Life. *ACS Appl. Mater. Interfaces* **2017**, *9*, 42717−42722.
(48) Qin, H.; Chen, L.; Wang, L.; Chen, X.; Yang, Z. V_2O_5 Hollow Spheres as High Rate and Long Life Cathode for Aqueous Rechargeable Zinc Ion Batteries. *Electrochim. Acta* **2019**, *306*, 307−316.
(49) Chen, D.; Rui, X.; Zhang, Q.; Geng, H.; Gan, L.; Zhang, W.; Li, C.; Huang, S.; Yu, Y. Persistent Zinc-Ion Storage in Mass-Produced V_2O_5 Architectures. *Nano Energy* **2019**, *60*, 171−178.
(50) Zhou, J.; Shan, L.; Wu, Z.; Guo, X.; Fang, G.; Liang, S. Investigation of V_2O_5 as a Low Cost Rechargeable Aqueous Zinc Ion Battery Cathode. *Chem. Commun.* **2018**, *54*, 4457−4460.
(51) Kundu, D.; Adams, B. D.; Duffort, V.; Vajargah, S. H.; Nazar, L. F. A high-Capacity and Long-Life Aqueous Rechargeable Zinc Battery Using a Metal Oxide Intercalation Cathode. *Nat. Energy* **2016**, *1*, 16119.
(52) Soundharrajan, V.; Sambandam, B.; Kim, S.; Alfaruqi, M. H.; Putro, D. Y.; Jo, J.; Kim, S.; Mathew, V.; Sun, Y.-K.; Kim, J. $Na_2V_6O_{16}\cdot 3H_2O$ Barnesite Nanorod: An Open-Door to Display a Stable and High-Energy for Aqueous Rechargeable Zn-Ion Batteries as Cathode. *Nano Lett.* **2018**, *18*, 2402−2410.
(53) Pang, Q.; Sun, C.; Yu, Y.; Zhao, K.; Zhang, Z.; Voyles, P. M.; Chen, G.; Wei, Y.; Wang, X. $H_2V_3O_8$ Nanowire/Graphene Electrodes for Aqueous Rechargeable Zinc Ion Batteries with High Rate Capability and Large Capacity. *Adv. Energy Mater.* **2018**, *8*, 1800144.

DOI: 10.1021/acsaem.9b01415
ACS Appl. Energy Mater. 2019, 2, 6904−6910